
THE **ASEAN** JOURNAL OF RADIOLOGY

Highlight

- Original Article
- Case Report
- ASEAN Movement
in Radiology
- Acknowledgement
of Reviewers

Official Journal of



The Royal College of Radiologists of Thailand,



ASEAN Association of Radiology, and



Foundation for Orphan and Rare Lung Disease

ASEAN
JOURNAL OF RADIOLOGY

ISSN 2672-9393

The ASEAN Journal of Radiology

Editor:	<i>Wiwatana Tanomkiat, M.D.</i>
Associate Editors:	<i>Pham Minh Thong, M.D., Ph.D.</i> <i>Narufumi Suganuma, M.D., Ph.D.</i> <i>Kwan Hoong Ng, Ph.D.</i> <i>Shafie Abdullah, M.D.</i> <i>Siriporn Hirunpat, M.D.</i> <i>Chang Yueh Ho, M.D.</i> <i>Maung Maung Soe, M.D.</i> <i>Kyaw Zaya, M.D.</i>
Assistant Editor:	<i>Nucharin Supakul, M.D.</i>
Statistical Consultant:	<i>Alan Frederick Geater, B.Sc., Ph.D.</i>
Language Consultant:	<i>Siriprapa Saparat, EIL</i>
Publishing Consultant:	<i>Ratchada Chalarat, M.A.</i>
Editorial Coordinator:	<i>Supakorn Yuenyongwannachot, B.A., M.Sc.</i>
Graphics:	<i>Kowa Saeooi, B.A.</i>
Publisher:	<i>Foundation for Orphan and Rare Lung Disease</i>

CONTENTS

03 From The Editor

05 Original Article

Abdominal CT radiation dose optimization at Siriraj Hospital (Phase III)

Piyaporn Apisarnthanarak, M.D.

Anawat Sriwaleephun, M.D.

Sastrawut Thammakittiphon, B.Sc., M.Sc.

Wimonrat Lornimitdee, B.Sc.

Atchariya Klinhom, RN.

Tarntip Suwatananonthakij, RN.

Kobkun Muangsomboon, M.D.

Wanwarang Teerasamit, M.D.

Sopa Pongpornsup, M.D.

Walailak Chaiyasoot, M.D.

20 Comparison of entrance surface air kerma measurement with MTS-N (LiF: Mg, Ti) chips with a kilovoltage X-ray source

Akintayo Daniel Omojola, M.Sc.

Samuel Olaolu Adeneye, Ph.D.

Michael Onoriode Akpochafor, Ph.D.

Isiaka Olusola Akala, M.Sc.

Azuka Anthonio Agboje, M.Sc.

35 Case Report

Mimicker of Fitz-Hugh-Curtis syndrome:

A case report of perihepatitis secondary to sigmoid colonic perforation

Sirote Wongwaisayawan, M.D.

Pinporn Jenjitranant, M.D.

Natthawut Jarunrarumol, M.D.

Goragoch Gesprasert, M.D., Ph.D.

Nitima Saksobhavit, M.D.

44 Pulmonary sclerosing pneumocytoma, an adenocarcinoma mimicker: A case report and review of the literature

Mohd Zulkimi Rosly, M.D.

Aida Widure Mustapha Mohd Mustapha, M.D.

Nik Farhan Nik Fuad, M.D.

55 ASEAN Movement in Radiology

The Royal College of Radiologists of Thailand in collaboration with Thailand Center of Excellence in Life Sciences shape the future of artificial intelligence in diagnostic radiology.

Sitthichok Chaichulee, Ph.D.

Thammasin Ingviya, M.D., Ph.D.

Supharek Thawillarp, M.D., D.P.H.

Pattarawin Attasara, M.D.

Wiwatana Tanomkiat, M.D.

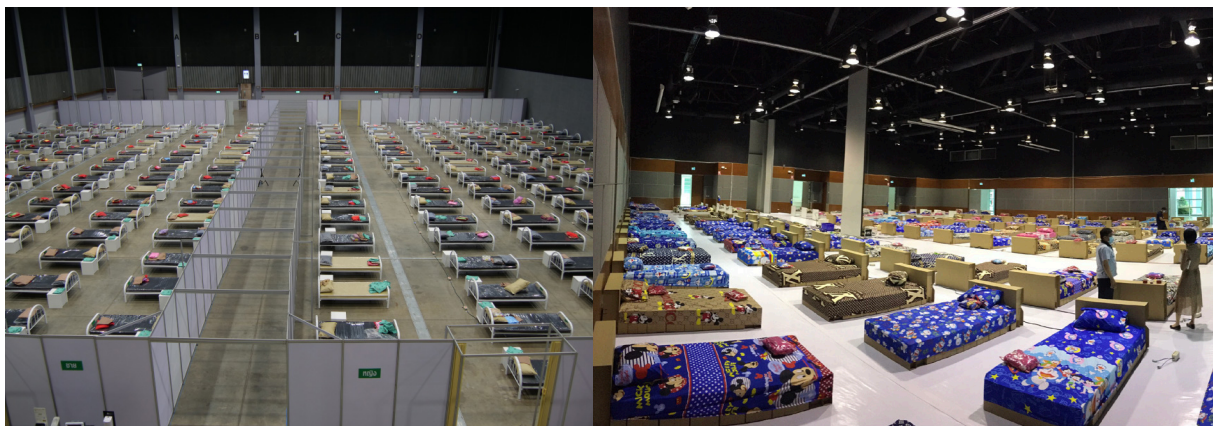
62 Acknowledgement of Reviewers

From The Editor

Received 20 April 2021; accepted 20 April 2021
doi:10.46475/aseanjr.v22i1.125

The third COVID-19 wave in Thailand

Thailand has faced the third wave of COVID19 since the first week of April. The first wave at the beginning of last year was from Chinese tourists, the second one at the end of last year from immigrants and Myanmar migrant laborers, but the source of the current wave remains unknown. It started with a group of young urban upper middle class people who got infected after visiting night clubs and restaurants at the heart of Bangkok during the long weekend, spreading the disease to their families and relatives and across the whole country. What is alarming is that it took less than two weeks to become widespread, much faster and wider than the two prior ones. It was that weekend and Qingming, the festival where relatives gather at their hometown in the certain lunar period once a year to show gratitude to their Chinese ancestors practiced widely in China, Eastern and Southeast Asia, to blame. Social distancing and mask wearing are not strictly observed, in fact impossible to do, in restaurants and night clubs where people drink, eat and chat for a couple of hours, not to mention in an air-conditioned room with low air circulation.



The top views inside the field hospitals (left) at Chiangmai, the most famous and significant province among tourists in the Northern Thailand [cited 2021 Apr 23]. Available from:<https://www.sanook.com/news/8362894/> and (right) at Songkla, the deep Southern Thailand.

To keep COVID-19 under control proves much more difficult this time as the infected cases are nationals, not tourists or migrant laborers. There are young middle class people in every career and sector; companies, factories, government offices, universities, service industries and even health services in hospitals. The government has declared the state of emergency thereof. It is by law that the suspected cases who are symptomatic, even with mild symptoms such as fever or a running nose, need to have a swab test done and are hospitalized once the test is revealed positive. There was no field hospital during the first wave, a few in a limited area of pandemic during the second wave, and everywhere this time.

Non-profit professional organizations in Radiology, including the Royal College of Radiologists of Thailand, the Thoracic Society of Thailand under Royal Patronage, the Thai Society of Radiological Technologists, the Radiological Society of Thailand, together with the Department of Medicine Services of the Ministry of Public Health, updated the practice guideline which was developed in the first wave. The core content is that imaging is not the sensitive test to detect COVID-19 infection. A chest radiograph should be performed only if the patient has symptoms and signs of pneumonia, to reveal the extent of disease involvement and to follow up. A CT is indicated only if other life-threatening conditions or comorbidities, such as pulmonary embolism or pneumothorax, are suspected. This is to reduce the unnecessary use of resources and workload.

Wiwatana Tanomkiat, M.D.

Editor,

The ASEAN Journal of Radiology

Email: aseanjournalradiology@gmail.com

Original Article

Abdominal CT radiation dose optimization at Siriraj Hospital (Phase III)

Piyaporn Apisarnthanarak, M.D.
Anawat Sriwaleephun, M.D.
Sastrawut Thammakittiphan, B.Sc., M.Sc.
Wimonrat Lornimitdee, B.Sc.
Atchariya Klinhom, RN.
Tarntip Suwatananonthakij, RN.
Kobkun Muangsomboon, M.D.
Wanwarang Teerasamit, M.D.
Sopa Pongpornsup, M.D.
Walailak Chaiyasoot, M.D.

From Department of Radiology, Faculty of Medicine Siriraj Hospital,
Mahidol University, Bangkok, Thailand.
Address correspondence to P.A. (e-mail: punpae159@gmail.com)

Received 28 August 2020; revised 5 April 2021; accepted 6 April 2021
doi:10.46475/aseanjr.v22i1.82

Abstract

Objective: To compare the image quality and the radiation dose between fixed tube current (FTC) low dose abdominal CT currently performed at our hospital and new automatic tube current modulation (ATCM) low dose abdominal CT.

Materials and Methods: We prospectively performed ATCM low dose abdominal CT in 88 participants who had prior FTC low dose CT for comparison. Four experienced abdominal radiologists independently and blindly assessed the quality of FTC and ATCM low dose CT images by using a 5-point-scale satisfaction score (1 = unacceptable, 2 = poor, 3 = average, 4 = good, and 5 = excellent image quality). Each reader selected the preferred image set between FTC and ATCM

low dose techniques for each participant. The image noise of the liver and the aorta in both techniques was measured. The volume CT dose index (CTDIvol) of both techniques was compared.

Results: The mean satisfaction scores (SD) for FTC and ATCM low dose CT were 4.38 (0.66) and 4.38 (0.64), respectively with the ranges of 3 to 5 in both techniques, which were all acceptable for CT interpretation. The preferred image set between FTC and ATCM low dose techniques of each participant randomly selected by each reader were varied, depending on the readers' opinions. The mean image noise of the aorta on FTC and ATCM low dose CT accounted for 34.75 and 36.46, respectively, while the mean image noise of the liver was 28.86 and 29.81, respectively. The mean CTDIvol (SD) of FTC and ATCM low dose CT were 8.42 (0.32) and 8.12 (0.43) mGy, respectively.

Conclusion: FTC and ATCM low dose abdominal CT provided comparable acceptable image quality and showed no clinical significance in radiation dose optimization.

Keywords: Abdominal computed tomography, Abdominal CT, Radiation dose optimization, Fixed tube current, FTC, Automatic tube current modulation, ATCM.

Introduction

Nowadays, the new computed tomography (CT) technologies have offered the better image qualities by providing thinner and faster CT images. Despite obtaining better image resolution and ability to achieve a dynamic study, CT comes along with more radiation dose, which is a worldwide concern as one of the potential risks of carcinogenesis [1]. There have been many proposed guidelines for radiation dose optimization, such as minimizing the number of CT acquisitions and area coverage, reducing the tube current, and decreasing peak kilovoltage [2,3] as appropriate. Two accepted techniques of tube current optimization include fixed tube current (FTC) and automatic tube current modulation (ATCM) techniques. FTC is easy to be performed, using a fixed, tube current reduction. ATCM is more complicated, using automatic adjustment of the tube current by a CT scanner according to the size and density of the scanned body part. Both techniques have provided radiation dose reduction with similar image quality [4-6].

However, radiation dose reduction unavoidably increases the image noise, reduces the image quality and decreases diagnostic confidence. For the aforementioned reasons, we have conducted the studies on tube current reduction by either FTC (phase I study) or ATCM (phase II study) techniques to find out the appropriate technique and the amount of tube current reduction and assess the post-processing reconstruction methods which help optimizing the image quality.

Our phase I study [7] was prospectively performed in 119 participants, comparing low dose abdominal CT using the FTC technique (30% reduction of standard tube current) and conventional standard dose CT. We applied the new iterative reconstruction (IR) de-noising method to optimize the image quality of the low dose CT scan. IR provided less image noise than the conventional filtered back projection (FBP) method and could help reduce the radiation dose [8-14]. The IR method used in the study was the Adaptive Statistical Iterative Reconstruction (ASiR), which was specific to our GE CT scanners. We applied various parameters of ASiR (0%, 10%, 20%, and 30%) by post-processing on a CT

workstation to improve the low dose CT image quality. The result of the phase I study showed significant radiation dose reduction by the FTC technique with acceptable image quality by the opinions of the four experienced abdominal radiologists.

Our phase II study [15] was prospectively performed in 111 participants, comparing low dose abdominal CT using the ATCM technique and conventional standard dose CT. The ATCM low dose CT images were post-processed on a CT workstation with 4 parameters of ASiR (0%, 10%, 20%, and 30%). The result of the phase II study also showed significant radiation dose reduction by the ATCM technique with acceptable image quality by the opinions of the four experienced abdominal radiologists.

The increment of ASiR technique was helpful in reducing image noise in phase I and phase II studies. However, the images with high percentage of ASiR provided smooth image appearances with a less sharp border. This was the reported major drawback of the IR technique [11,13]. Half of the radiologists in our phase I and phase II studies preferred CT images with lower percentage of ASiR than higher percentage of ASiR. They were possibly familiar with relatively noisy CT images with a sharp border in lower percentage ASiR.

According to the results of phase I and phase II studies, we have applied FTC technique to reduce the radiation dose in our routine CT practice. We selected the FTC technique because it is simple and easy to be performed compared to the more complicated ATCM technique. We decided to fixedly reduce the tube current by 20%, from 400 to 300 mA on a 64-slice CT scanners and from 340 to 250 mA on a 256-slice CT scanner (standard mA multiplied with mA adjustment factor for 20 % dose reduction of 0.76 and 0.74 for 64-slice and 256-slice CT scanners, respectively). We do not apply the ASiR method in our routine practice due to different radiologists' preference as described above. In this current phase III study, we aimed to directly compare the image quality and the radiation dose between the two techniques of tube current optimization; the FTC technique which has currently been used as our routine practice and the ATCM technique.

Materials and methods

Study Designs and Participants

This study was a prospective, single-centered study performed at a 2,200-bed university hospital in central Thailand. This study was approved by our institutional review board with informed consents required from all included participants.

All participants were over 18 years old who were scheduled for contrast enhanced abdominal CT examinations at our department. They had available prior FTC low dose abdominal CT which has been currently used in our department for the comparison purpose with their current CT using the ATCM low dose technique. Totally, eighty-eight participants met the criteria and were recruited as our study population. The demographic data of each participant including gender and age were recorded by one of our investigators (AS).

CT Techniques

FTC Low Dose Abdominal CT

The prior FTC low dose abdominal CT of our participants was routinely performed by three General Electric (GE) CT scanners including two 64-slice scanners (Discovery CT750 High Definition, GE Healthcare, Milwaukee, WI, USA) and one 256-slice scanner (Revolution CT, GE healthcare, Milwaukee, WI, USA). The CT of each participant was protocolled for a proper number of CT acquisitions and area coverage. All participants were advised to hold their breath during the scan. The scan coverage included at least the upper abdominal area. The slice collimation was 1.25 mm (reconstructed at 7.0 mm) for all scanners. There were varieties on the administration of oral and rectal contrasts according to each participant's appropriate protocol. All participants underwent precontrast and postcontrast studies, before and after a bolus intravenous injection of nonionic iodinated contrast agent (2 mL per kg body weight), followed by 20 mL of water via a power injector at a rate of 3 mL/second. Each participant had at least a portovenous acquisition phase with an 80-second delay for postcontrast study. An additional arterial phase at 35 to 40-second delay or delayed phase at a 5 to 10-

minute delay was obtained in some participants as necessary. The peak kilovoltage was fixed at 120 kVp for all scanners. The tube current of our FTC technique was 300 mA and 250 mA for 64-slice and 256-slice CT scanners, respectively. The rotation time was 0.5 second for all scanners. The pitch was 1.375:1 and 0.992:1 for 64-slice and 256-slice CT scanners, respectively. All images were reconstructed with the standard FBP without the addition of ASiR, and sent to the Picture Archiving and Communication System (PACS) for subsequent reviews.

ATCM Low Dose Abdominal CT

The current ATCM low dose abdominal CT was performed by two GE CT scanners including one 64-slice scanner (Discovery CT750 High Definition, GE Healthcare, Milwaukee, WI, USA) and one 256-slice scanner (Revolution CT, GE healthcare, Milwaukee, WI, USA). The CT scanners for the FTC and ATCM techniques of each participant were not necessarily the same scanners. The CT of each participant was protocolled for a proper number of CT acquisitions and area coverage which at least covered the upper abdominal area. The scan techniques were the same as described in the prior FTC low dose abdominal CT protocol except for the tube current on the portovenous phase was automatically adjusted by the CT scanners according to the size and density of each participant's abdomen. The tube current varied between 150-300 mA with a fixed noise index of 22 on a 64-slice CT scanner; and 120-250 mA with a fixed noise index of 22 on a 256-slice CT scanner. The other phases used the FTC technique as a routine (300 and 250 mA for 64-slice and 256-slice CT scanners, respectively). We chose to study only the portovenous phase because most abdominal organs had homogeneous enhancement in this phase. It was easy for radiologists to evaluate the CT image quality.

All images were reconstructed with the standard FBP without the addition of ASiR, and sent to PACS for subsequent reviews.

For a parameter of radiation dose comparison, we selected the volume CT dose index (CTDI_{vol}) instead of the dose length product (DLP). The DLP would depend on the length of scan which varied among the participants due to the difference in area coverage and the number of CT acquisitions.

The details of CT scanners, study dates, and CTDIvol in the portovenous phase of each participant's prior FTC low dose abdominal CT and current ATCM low dose abdominal CT were recorded by one of our investigators (AS). The time interval between the two studies was calculated.

Image Assessment

In the qualitative image assessment, four board-certified, abdominal radiologists (PA, KM, WT, and SP with 24, 24, 18, and 18 years of experience in abdominal CT evaluation) blindly reviewed portovenous abdominal CT image sets of the FTC and the ATCM techniques of each participant. They separately graded the image quality of both low dose techniques by using a 5-point-scale satisfaction score on a visual scale as follows:

- 1: Unacceptable image quality, unable to interpret
- 2: Poor image quality, interfering with interpretation
- 3: Average image quality, possible interpretation
- 4: Good image quality
- 5: Excellent image quality

The satisfaction scores of 3 to 5 were acceptable for CT interpretation. Subsequently, the radiologists independently selected one preferred image set between the FTC and the ATCM techniques for each participant.

In the quantitative image assessment, the image noise (HU) of the aorta and the liver was measured on FTC and ATCM low dose CT image sets by one of our investigators (AS) on a CT workstation (Advantage workstation AW 4.6, GE healthcare, Milwaukee, WI, USA). The image noise was measured by drawing a circular region of interests (ROIs) at four locations (one aortic and three hepatic regions) on a 1.25-mm slice portovenous image at the same locations and levels of these two image sets. For image noise of the aorta, the ROI was drawn at the most central part to avoid calcified plaque at the aortic wall. For image noise of the liver, three hepatic ROIs were routinely applied on the left lobe, the anterior right lobe, and the posterior right lobe (Figure 1). The hepatic ROIs were placed

at the homogenous enhancing hepatic areas avoiding vessels, bile ducts, hepatic lesions, calcifications and surgical materials. The mean image noise of each liver was calculated from these three hepatic ROIs of image noise. The area of aortic and hepatic ROIs was in a range of 93-106 mm², mean 100.5 mm² ± 2.92mm².

Statistical Analysis

The demographic data of participants, CT scanners, time interval between CT studies, the image quality (satisfaction scores, readers' preferred low dose techniques, and image noise) and CTDIvol of FTC and ATCM low dose CT were presented as percentage (%), mean (standard deviation, SD), and range. A paired t-test was used to compare the mean CTDIvol and the mean image noise of the aorta and the liver between the FTC and the ATCM low dose CT.

All statistical data analyses were performed by using PASW 18.0 (SPSS Inc., Chicago, IL, USA). A 2-sided p-value of less than or equal to 0.05 was considered as a statistical significance.



Figure 1. The image noise measurement of the aorta (1 ROI) and the liver (3 ROIs at the left lobe, the anterior right lobe and the posterior right lobe). The ROIs were positioned at the same locations and levels on FTC and ATCM image sets.

Results

Participants

Eighty-eight participants in this study included 46 (52.3%) men and 42 (47.7%) women. The mean age (SD) of the participants at the time of the ATCM low dose CT scan was 62.5 (12.1) years with the range of 21-86 years.

CT Techniques

The FTC low dose abdominal CT of 50 (56.8%) and 38 (43.2%) participants were performed by 64-slice and 256-slice scanners, respectively. The ATCM low dose abdominal CT of 56 (63.6%) and 32 (36.4%) participants were performed by 64-slice and 256-slice scanners, respectively. The time interval between the two studies ranged from 38 to 208 days (median 133 days).

The mean CTDI_{vol} (SD) of the FTC and the ATCM low dose CT were 8.42 (0.32) and 8.12 (0.43) mGy, respectively (p-value <0.001).

Image Assessment

In terms of the qualitative image assessment, the satisfaction score of the FTC and the ATCM low dose abdominal CT graded by four readers ranged from 3 to 5, which were all acceptable for CT interpretation. The mean satisfaction scores of FTC and ATCM low dose abdominal CT graded by each reader were summarized in Table 1. The preferred image set between the FTC and the ATCM low dose techniques of each participant randomly selected by each reader were varied, depending on the readers' opinions (Table 2).

In the quantitative image assessment, the image noise of the aorta and the liver on the FTC and the ATCM low dose abdominal CT were summarized in Table 3.

Table 1. The mean satisfaction scores of the FTC and the ATCM low dose abdominal CT graded by four readers.

	Mean Satisfaction Score (SD)	
	FTC	ATCM
Reader1	4.24 (0.77)	4.24 (0.70)
Reader2	4.47 (0.57)	4.43 (0.54)
Reader3	4.48 (0.61)	4.56 (0.62)
Reader4	4.34 (0.68)	4.33 (0.64)
All reader	4.38 (0.66)	4.38 (0.64)

Table 2. The preferred image set between the FTC and the ATCM techniques selected by 4 readers.

	Number of Preferred Image Set (%)		Total
	FTC	ATCM	
Reader1	38 (43.2)	50 (56.8)	88 (100.0)
Reader2	48 (54.5)	40 (45.5)	88 (100.0)
Reader3	33 (37.5)	55 (62.5)	88 (100.0)
Reader4	37 (42.0)	51 (58.0)	88 (100.0)
All reader	156 (44.32)	196 (55.68)	352 (100.0)

Table 3. The image noise (HU) of the aorta and the liver on the FTC and the ATCM low dose abdominal CT.

		FTC	ATCM	Differences of Mean Image Noise between FTC and ATCM (95% CI)	p-Value
		Aorta	Mean (SD)	34.75 (7.28)	36.46 (7.72)
	Min, Max	21.78, 55.12	22.88, 53.71		
Liver	Mean (SD)	28.86 (6.38)	29.81 (5.94)	-0.95 (-1.59,-0.31)	0.004
	Min, Max	12.03, 52.84	14.90, 53.71		

Discussion

From our previous phase I [7] and phase II [15] studies, both FTC and ATCM low dose abdominal CT provided significant radiation dose reduction compared to the standard dose CT, and at the same time offered acceptable image quality. The purpose of this current phase III study was to directly compare these two aforementioned low dose CT techniques in either image quality or radiation dose.

The result of this study showed no clinically significant difference in the image quality between the FTC and the ATCM low dose abdominal CT, similar to the findings shown in prior studies [5,6]. Both techniques demonstrated acceptable satisfaction scores for interpretation ranging from 3 to 5. Interestingly, the mean satisfaction score of the FTC and the ATCM were similar (4.38), but the number of the preferred study selected by readers was slightly higher on the ATCM (55.68%) compared to the FTC (44.32%) techniques. These could be explained in cases when the readers gave the same satisfaction score for both techniques but selected one of them to be a preferred study. The mean satisfaction score would possibly not go along with the number of preferred studies as shown in our result.

The radiation dose of the FTC technique in this study was slightly higher than the ATCM technique with statistical significance (CTDIvol of 8.42 vs 8.12 with p-value <0.001). As mentioned earlier that the ATCM technique automatically adjusted the tube current according to the size and density of the scanned body part, the radiation dose in the ATCM technique was more suitable with each participant than the FTC technique [5,6]. Nevertheless, the difference in a radiation dose of these two techniques was not clinically significant. With slightly more radiation dose, the FTC technique did show less image noise of the aorta and the liver compared to the ATCM technique.

From our experiences performing 3 consecutive studies with a low dose abdominal CT, we assured that a low dose abdominal CT with an optimal technique and an appropriate amount of radiation reduction would provide CT images with an acceptable quality. Radiologists should be concerned about radiation hazard and

realize the importance of radiation dose optimization. They have to open their mind to adopt low dose CT images with acceptable quality in their routine work. There are many proposed techniques of radiation dose optimization. They just select the technique that is most suitable with their CT machines and radiological practice.

There were several limitations of our study. First, there were variables in our CT scanners. Although they were all GE scanners, two were 64-slice scanners and one was a 256-slice scanner. Of which, some CT parameters (i.e. mA and pitch) were not the same. Inherent differences in scanners could affect the image quality. Plus, the CT scanners for the FTC and the ATCM techniques of each participant were not necessarily the same scanners. Second, the long interval time between the prior FTC low dose CT and current ATCM low dose CT ranged from 38 to 208 days (median 133 days). With such a long interval time, there would be changes in participants' habitus or conditions that would affect the image quality. Third, image noise was measured on a 1.25 mm slice portovenous image of each image set. As a matter of fact, image noise should be measured by choosing 3-5 consecutive CT slices and the noise should be averaged for the statistical accuracy. Lastly, our study focused only on the image quality (satisfaction score, preferred image set, and image noise). We did not study diagnostic performances of these low dose techniques. To accurately evaluate the diagnostic performances between the 2 techniques, these 2 techniques should be performed on the same date and almost the same acquisition phase. These will inevitably increase the radiation dose received by the participants.

In conclusion, the FTC low dose abdominal CT and the ATCM low dose abdominal CT provided a comparable acceptable image quality, and demonstrated no clinical significance in radiation dose optimization.

References

1. Hall EJ, Brenner DJ. Cancer risks from diagnostic radiology: the impact of new epidemiological data. *Br J Radiol* 2012;85:e1316-7. doi: 10.1259/bjr/13739950.
2. Hara AK, Wellnitz CV, Paden RG, Pavlicek W, Sahani DV. Reducing body CT radiation dose: beyond just changing the numbers. *AJR Am J Roentgenol* 2013;201:33-40. doi: 10.2214/AJR.13.10556.
3. Tamm EP, Rong XJ, Cody DD, Ernst RD, Fitzgerald NE, Kundra V. Quality initiatives: CT radiation dose reduction: how to implement change without sacrificing diagnostic quality. *RadioGraphics* 2011;31:1823-32. doi: 10.1148/rg.317115027.
4. Kalra MK, Maher MM, Toth TL, Schmidt B, Westerman BL, Morgan HT, et al. Techniques and applications of automatic tube current modulation for CT. *Radiology* 2004;233:649-57. doi: 10.1148/radiol.2333031150.
5. Kalra MK, Maher MM, Toth TL, Kamath RS, Halpern EF, Saini S. Comparison of Z-axis automatic tube current modulation technique with fixed tube current CT scanning of abdomen and pelvis. *Radiology* 2004;232:347-53. doi: 10.1148/radiol.2322031304.
6. Lee S, Yoon SW, Yoo SM, Ji YG, Kim KA, Kim SH, et al. Comparison of image quality and radiation dose between combined automatic tube current modulation and fixed tube current technique in CT of abdomen and pelvis. *Acta Radiol* 2011;52:1101-6. doi: 10.1258/ar.2011.100295.
7. Apisarnthanarak P, Buranont C, Boonma C, Janpanich S, Suwatananonthakij T, Klinhom A, et al. Abdominal CT radiation dose optimization at Siriraj Hospital. *ASEAN J Radiol* 2020;21(2):28-43.

8. Patino M, Fuentes JM, Singh S, Hahn PF, Sahani DV. Iterative reconstruction techniques in abdominopelvic CT: technical concepts and clinical implementation. *AJR Am J Roentgenol* 2015;205:W19-31. doi: 10.2214/AJR.14.13402.
9. Willemink MJ, de Jong PA, Leiner T, de Heer LM, Nievelstein RA, Budde RP, et al. Iterative reconstruction techniques for computed tomography Part 1: technical principles. *Eur Radiol* 2013;23:1623-31. doi: 10.1007/s00330-012-2765-y.
10. Geyer LL, Schoepf UJ, Meinel FG, Nance JW Jr, Bastarrika G, Leipsic JA, et al. State of the art: iterative CT reconstruction techniques. *Radiology* 2015;276:339-57. doi: 10.1148/radiol.2015132766.
11. Mitsumori LM, Shuman WP, Busey JM, Kolokythas O, Koprowicz KM. Adaptive statistical iterative reconstruction versus filtered back projection in the same patient: 64 channel liver CT image quality and patient radiation dose. *Eur Radiol* 2012;22:138-43. doi: 10.1007/s00330-011-2186-3.
12. Prakash P, Kalra MK, Kambadakone AK, Pien H, Hsieh J, Blake MA, et al. Reducing abdominal CT radiation dose with adaptive statistical iterative reconstruction technique. *Invest Radiol* 2010;45:202-10. doi: 10.1097/RLI.0b013e3181dzfeec.
13. Sagara Y, Hara AK, Pavlicek W, Silva AC, Paden RG, Wu Q. Abdominal CT: comparison of low-dose CT with adaptive statistical iterative reconstruction and routine-dose CT with filtered back projection in 53 patients. *AJR Am J Roentgenol* 2010;195:713-9. doi: 10.2214/AJR.09.2989.
14. Gervaise A, Osemont B, Louis M, Lecocq S, Teixeira P, Blum A. Standard dose versus low-dose abdominal and pelvic CT: comparison between filtered back projection versus adaptive iterative dose reduction 3D. *Diagn Interv Imaging* 2014;95:47-53. doi: 10.1016/j.diii.2013.05.005.

15. Apisarnthanarak P, Hongpinyo S, Saysivanon K, Boonma C, Janpanich S, Ketkan P, et al. Abdominal CT radiation dose optimization at Siriraj Hospital (Phase II). ASEAN J Radiol 2020;21(3):5-24. doi: <https://doi.org/10.46475/aseanjr.v21i3.81>

Original Article

Comparison of entrance surface air kerma measurement with MTS-N (LiF: Mg, Ti) chips with a kilovoltage X-ray source

Akintayo Daniel Omojola, M.Sc.⁽¹⁾

Samuel Olaolu Adeneye, Ph.D.⁽²⁾

Michael Onoriode Akpochafor, Ph.D.⁽²⁾

Isiaka Olusola Akala, M.Sc.⁽³⁾

Azuka Anthonio Agboje, M.Sc.⁽¹⁾

From ⁽¹⁾Department of Radiology, Medical Physics Unit, Federal Medical Centre Asaba, Delta State, Nigeria.

⁽²⁾Department of Radiation Biology, Radiotherapy and Radiodiagnosis, College of Medicine, University of Lagos, Lagos State, Nigeria.

⁽³⁾Department of Radiology, Lagos University Teaching Hospital, Ikeja, Lagos, Lagos State, Nigeria.

Address correspondence to A.D.O. (e-mail: akintayo.omojola@fmcasaba.org)

Received 30 November 2020; revised 10 February 2021; accepted 18 March 2021
doi:10.46475/aseanjr.v22i1.96

Abstract

Objective: Radiation detectors are key components that ensure the accuracy and performances of dosimetry equipment. The study is aimed to compare the mean entrance surface air kerma (ESAK) between a DCT-100mm ionization chamber (IC) and MTS-N (LiF: Mg, Ti) chips when both detectors are exposed to $\leq 5\text{mGy}$ with a 10 by 10 field size, with an X-ray source and to determine the accuracy of the Thermoluminescent (TL) chips. Also, the dose will be compared to similar studies.

Materials and Methods: A functional, Digital Radiography (DR) X-ray System was used. A DCT-100mm ionization chamber (IC) and an XR Multidetector was positioned at a Source to Image Distance (SID) of 100cm on polystyrene, about 20cm thick. An X-ray spectrum generated at a Practical Peak Voltage (PPV) of 60-107kV with Half Value Layer (HVL) of 2.4-4.3mmAl and filtration > 3mmAl was used. The same setup was used for the MTS-N chips.

Results: The mean doses for 1-5 mGy with the MTS-N chips were 1.07 ± 0.07 , 1.60 ± 0.13 , 2.23 ± 0.11 , 2.58 ± 0.07 and 3.45 ± 0.10 mGy respectively, with accuracies of 7, 20, 26, 36 and 31%. Dose accuracy at 1 and 2mGy was within 25% respectively. Dose accuracies at 3, 4 and 5mGy was within >25%. The correction factor for 1-5mGy was 0.94, 1.25, 1.35, 1.55 and 1.45 respectively.

Conclusion: Validation of the MTS-N chips with the reference ionization chamber to this study was within 36%. The Radiation and Nuclear Safety Authority (STUK) recommends that ESAK be within 25% for entrance surface dose. ESAK accuracy mostly increased with dose as observed in this study.

Keywords: Entrance surface air kerma, Backscatter radiation, Accuracy, Ionization chamber, Detector, MTS-N chips.

Introduction

Diagnostic medical exposure accounts for the largest use of ionizing radiation globally [1-3]. The cost of doing a routine X-ray examination is considered the cheapest, compared to other imaging modalities. Today, patient dosimetry plays an important role in dose optimization, intending to protect patients from an unusual high radiation dose [4-6]. Today in Nigeria, there is no patient dose audit in most diagnostic radiology facilities due to the lack of manpower (medical physicist) and dosimetric tools for dose assessment [7].

An important document titled dosimetry in diagnostic radiology: An international code of practice published by the International Atomic Energy Agency (IAEA), under the technical reports series no. 457 has been adopted as a guide in determining uncertainty associated with the use of thermoluminescent dosimeters (TLDs) and other dose indicators for patient dosimetry [8]. Materials like Lithium Fluoride (LiF) doped with Magnesium (Mg) and Titanium (Ti) are the most widely used for this purpose because of their density and tissue-equivalent nature [9-11]. Most new radiographic systems, now come with parallel plate IC for dose measurements over a certain beam area, for patient dose assessment [12]. The energy response of TLDs particularly LiF: Mg, Ti have been studied for personal and patient dosimetry, with a minimum detectable dose of 0.01mSv [13, 14].

The principal quantities for patient dosimetry in general radiography are the incident air kerma (iAK), the entrance surface air kerma (ESAK) and the air kerma–area product (AKAP). One or more of these quantities may be determined depending upon user requirements. The ESAK measurement can be done indirectly or directly. The indirect method requires no patient but the direct method requires the presence of a patient. In either case, TLDs have the advantage of being physically small, enabling them to be placed or attached to the body of the patient with ease, with very little interference in patient mobility or comfort and they are unlikely to obscure useful diagnostic information. Direct dose measurements during the course of real examinations on real patients provide the best indication of actual clinical practice [15, 16].

This study used MTS-N (LiF: Mg, Ti) chips. General use of TLDs requires that they are first annealed to erase residual energy using an annealing oven at known temperatures, after which they are exposed to ionizing radiation before they are read using a TLD reader. Usually, the measurement chamber of the reader contains a PMT Tube module, a heating unit, an exchangeable filter unit and a nitrogen gas supply unit. Once the element is heated through the heating unit, trapped energy is released in the form of light, from which a Photo Multiplier Tube (PMT) does the light amplification before it is converted into an electrical signal [17].

In a facility where MTS-N chips are newly available for patient dose audit, the accuracy of these chips is of great concern to avoid dose errors; hence, the purpose of this study was to compare the mean ESAK between a DCT-100mm Ionization Chamber (IC), which will serve as our reference instrument and MTS-N (LiF: Mg, Ti) chips. Both detectors will be exposed to 1, 2, 3, 4 and 5mGy respectively, under the same condition to determine the accuracy that exists between both devices.

Materials and methods

A Digital X-ray unit with acceptable exposure reproducibility was used. The calibrated DCT-100mm Ionization Chamber (IBA Dosimetry, Germany) was used alongside a MagicMax basic unit, which can measure doses (in μGy , mGy and Gy) and other quantities like the dose rate and exposure time simultaneously. The IC was carefully placed on a rectangular polystyrene material. It was positioned at a Source to Image Distance (SID) of 100cm, covering a beam area of 10 by 10 cm^2 . These processes were used alongside the XR Multi-Detector, which is a semiconductor, which can measure the dose (mGy), Practical Peak Voltage (PPV), Half Value Layer (HVL) and beam filtration. Exposure was made within the range of 60-107kV to achieve 1-5mGy. The range of HVL was 2.4-4.3mm, using the MagicMax XR detector (RQA-5). The same set-up as mentioned above was used for the pre-annealed MTS-N chips, with the size of 3.2mm \times 3.2mm \times 0.9mm (Figure 1). A RadPro Cube 400 manual TLD Reader (Freiberg Instruments GmbH, Germany) was used to determine corresponding TL count for the chips. The average background count was obtained from several TL chips that were not exposed to radiation denoted as TL_0 . The obtained TL counts ($\text{TL}_i - \text{TL}_0$) were multiplied with a pre-determined X-ray calibration factor [18]. The equation was as follows [8]:

$$ESAK = (TL_i - TL_0) \times CF_{CS-137} \left(\frac{mGy}{count} \right) \quad [1]$$

Where $TL_i=1, 2, 3\dots$ is the count from the ten selected chips, TL_0 is the background count, and CF is the Calibration Factor for Cesium-137 source. This study compared % deviation between measured and actual ESAK. The percentage deviation and absolute error were given as:

$$\% \text{ Deviation} = \frac{D_{measured} - D_{actual}}{D_{actual}} \quad [2]$$

Where:

$D_{measured}$ = was the dose obtained with the MTS-N chips

D_{actual} = was the dose obtained with the DCT-100mm Ionization Chamber

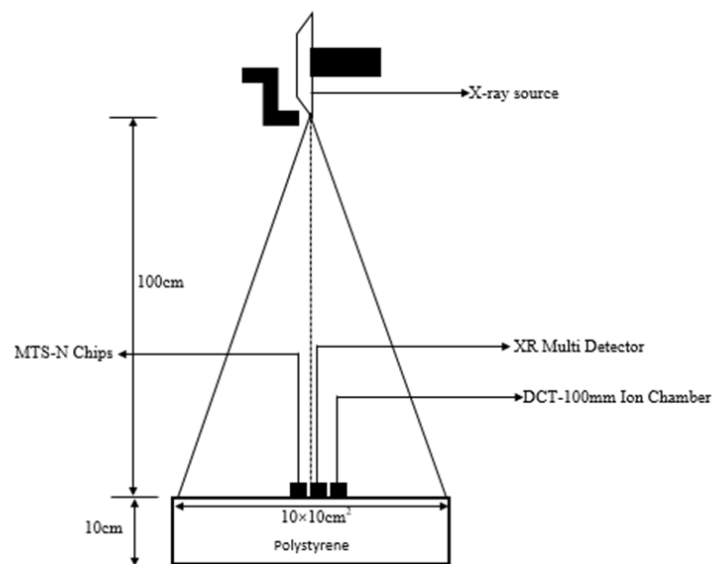


Figure 1. Setup for the measurement of ESAK with ionization chamber (the MTS-N chips were arranged in this manner and numbered serially).

Results

The mean measured ESAK with the MTS-N chips at 1mGy was 1.07 ± 0.07 mGy with a deviation of 7%. The % deviation of the individual MTS-N chips was 14, 17, 3, 8, 9, 4, -5, 16, 6 and -1 respectively, with the highest from the second TL chip. The absolute error (Ea) ranged from 0.01-0.17 (Table 1).

Table 1. Comparison of the actual and measured dose at 1 mGy.

No of chips	Measured dose (mGy)	Actual dose (mGy)	Absolute error (Ea)
1	1.14	1	0.14
2	1.17	1	0.17
3	1.03	1	0.03
4	1.08	1	0.08
5	1.09	1	0.09
6	1.04	1	0.04
7	0.95	1	0.05
8	1.16	1	0.16
9	1.06	1	0.06
10	0.99	1	0.01

Also, the mean measured ESAK with the MTS-N chips at 2mGy was 1.59 ± 0.13 mGy with a deviation of 20%. The % deviation of the individual MTS-N chips was -11.5, -24.5, -29, -13.5, -18.5, -27.5, -26, -12.5, -22 and -20.5 respectively. The absolute error (Ea) ranged from 0.23-0.58, with the highest deviation from the third chip (Table 2).

Table 2. Comparison of the actual and measured dose at 2 mGy.

No of chips	Measured dose (mGy)	Actual dose (mGy)	Absolute error (Ea)
1	1.77	2	0.23
2	1.51	2	0.49
3	1.42	2	0.58
4	1.73	2	0.27
5	1.63	2	0.37
6	1.45	2	0.55
7	1.48	2	0.52
8	1.75	2	0.25
9	1.56	2	0.44
10	1.59	2	0.41

Furthermore, the mean measured dose with the MTS-N chips at 3mGy was 2.23 ± 0.11 mGy with a deviation of 26%. The % deviation from individual MTS-N chips were -25, -22, -31, -20, -28, -25, -31, -23, -26 and -26 respectively. The absolute error (Ea) ranged from 0.61-0.94 (Table 3).

Table 3. Comparison of the actual and measured dose at 3 mGy.

No of chips	Measured dose (mGy)	Actual dose (mGy)	Absolute error (Ea)
1	2.25	3	0.75
2	2.35	3	0.65
3	2.06	3	0.94
4	2.39	3	0.61
5	2.16	3	0.84
6	2.26	3	0.74
7	2.08	3	0.92
8	2.32	3	0.68
9	2.22	3	0.78
10	2.23	3	0.77

Also, the mean measured dose with the MTS-N chips at 4mGy was 2.58 ± 0.07 mGy with a deviation of 36%. The % deviation from individual MTS-N chips were -13, -17, -11, -14, -11, -10, -13, -12, -15 and -9 respectively. The absolute error (Ea) ranged from 0.35-0.66 (Table 4).

Table 4. Comparison of the actual and measured dose at 4 mGy.

No of chips	Measured dose (mGy)	Actual dose (mGy)	Absolute error (Ea)
1	3.48	4	0.52
2	3.34	4	0.66
3	3.56	4	0.44
4	3.46	4	0.54
5	3.58	4	0.42
6	3.6	4	0.40
7	3.48	4	0.52
8	3.52	4	0.48
9	3.4	4	0.60
10	3.65	4	0.35

Finally, the overall average measured dose with the MTS-N chips at 5mGy was 3.45 ± 0.10 mGy with a deviation of 31%. The % deviation from individual MTS-N chips were -32.4, -32.2, -29.0, -32.6, -27.4, -28.4, -31.6, -32.4, -32.6, and -30.6 respectively. The absolute error (Ea) ranged from 1.37-1.63 (Table 5).

Table 5. Comparison of the actual and measured dose at 5 mGy.

No of chips	Measured dose (mGy)	Actual dose (mGy)	Absolute error (Ea)
1	3.38	5	1.62
2	3.39	5	1.61
3	3.55	5	1.45
4	3.37	5	1.63
5	3.63	5	1.37
6	3.58	5	1.42
7	3.42	5	1.58
8	3.38	5	1.62
9	3.37	5	1.63
10	3.47	5	1.53

Discussion

This study determined surface doses using an X-ray source in the range of 60-107kV from which 1-5mGy was achieved. Deviation in dose progressively increased from 1-3mGy. Dose at 1mGy was the most accurate (7%) due to the small influence of the backscatter radiation (BSR) compared to doses from 2-5mGy. The highest deviation was observed with 4mGy, which was 36%. Although correction factors were determined concerning the actual dose that was delivered, which ranged from 0.94-1.55, the radiation and nuclear safety authority guideline (STUK) in Finland recommends that the entrance surface air kerma (ESAK) be within $\pm 25\%$. Compared with our study, it shows that only 1 and 2 mGy were within the recommended limit. We observed that the ESAK from the IC may increase, due to the influence of scatter radiation as a result of the size and shape of the chamber relative to the ESAK from the TL chips, thereby by increasing the deviation. The latter may be prominent as dose increases (3-5mGy).

A study by Nilsson and Sorcini also reported the use of some correction factors of 0.82, 0.90 and 1.00 using a Cobalt-60 source with 6 and 21-MV in a study to determine surface dose measurements in clinical photon beams with TLDs [20].

Furthermore, a study by Yuosof et al, who compared the variation in dose between ionization chamber and TLD-100 shows that at 81 and 125kV, % deviation between the ionization and TLD-100 were 48 and 34% respectively. Similarly, with 6 and 10MV, % deviation was 19 and 18% respectively. The obtained results from their study for X-ray energy were similar to what we obtained for 60-107kV, which was $\pm 36\%$. The latter shows that at higher energies (radiotherapy range), better stability was observed [21].

High deviations at low doses using different types of TLDs have been reported. For instance, an investigation to the effect of TLD-700 energy response at low energy X-ray encountered in diagnostic radiology using caesium-137 source by Herrati et al, shows that maximum deviation could reach 60% and his study also shows that with the use of appropriate radiation quality (RQR5), dose accuracy can be reduced by up to 20% [22]. Alashrah et al in his study also reported a deviation up to 50% at the surface of a water phantom at a depth of 0.007cm as recommended by the International Commission on Radiological Protection (ICRP) and the International Commission on Radiation Units and Measurement (ICRU) with radiochromic films (RFs), thermoluminescent dosimeters and an ionization chamber with a 6-MV photon beam [23]. A study by Reynolds et al, who investigated surface dose using a 6MV X-ray beam shows a deviation of 27.72 and 41.92 with TLD and optically stimulated dosimeter (OSLD) for uncorrected doses [24]. Comparison of dosimeter response of the ionization chamber, TLD, and Gafchromic EBT2 film from a study by Fitriandini et al, shows that the accuracy associated with the use of TLD was -13.3% for surface dose in 3D-CRT, IMRT and SBRT. The maximum deviation in this study was $\pm 36\%$, [25].

Some other studies determined doses at certain depths. A study by Waqar et al reported an accuracy that was within 5% for a dose range of 250-5000mGy at a depth of 5cm [26], while Lee et al reported accuracy of 3% [27]. Measurement at a certain depth has been shown to deviate less compared to what was obtained in our study for entrance surface doses. As discussed above, a correction factor is often applied to compensate for this error.

Conclusion

A comparison of mean ESAK between IC and MTS-N chips using kilovoltage X-ray source was determined. The maximum deviation from the study was $\pm 36\%$. Better accuracy was obtained at a relatively lower dose (1 and 2 mGy), which was within $\pm 25\%$ as recommended in the Radiation and Nuclear Safety Authority (STUK); Helsinki, Finland, report for entrance surface dose. The determined correction factors show that there exist uncertainties, which may have affected measurements considering the size and shape of the detectors used. The study proves useful for patient dosimetry and will serve as a guide in diagnostic radiology.

Limitation of the study

1. The shape and thickness of the IC and the XR multi-detector may have increased scatter radiation compared to the MTS-N chip, which is relatively small.
2. Uncertainties arising from the TL chip was not factored in our calculations, which may have affected the accuracy of our results.

References

1. Do KH. General principles of radiation protection in fields of diagnostic medical exposure. *J Korean Med Sci* 2016;31 Suppl 1 :S6-9. doi: 10.3346/jkms.2016.31.S1.S6.
2. Awosan KJ, Ibrahim M, Saidu SA, Ma'aji SM, Danfulani M, Yunusa EU, et al. Knowledge of radiation hazards, radiation protection practices and clinical profile of health workers in a teaching hospital in Northern Nigeria. *J Clin Diagn Res* 2016; 10(8): LC07-12. doi: 10.7860/JCDR/2016/20398.8394.
3. Mettler FA Jr, Thomadsen BR, Bhargavan M, Gilley DB, Gray JE, Lipoti JA, et al. Medical radiation exposure in the U.S. in 2006: preliminary results. *Health Phys* 2008; 95: 502-7. doi: 10.1097/01.HP.0000326333.42287.a2.
4. Siström CL, McKay NL. Costs, charges, and revenues for hospital diagnostic imaging procedures: differences by modality and hospital characteristics. *J Am Coll Radiol* 2005;2:511-9. doi: 10.1016/j.jacr.2004.09.013.
5. Bercovich E, Javitt MC. Medical imaging: from roentgen to the digital revolution, and beyond. *Rambam Maimonides Med J* 2018;9(4):e0034. doi: 10.5041/RMMJ.10355.
6. Howell JD. Early clinical use of the X-ray. *Trans Am Clin Climatol Assoc* 2016; 127:341-9.
7. Obed RI, Ekpo ME, Omojola AD, Abdulkadir MK. Medical physics professional development and education in Nigeria. *Med Phys Int* 2016;4: 96-8.
8. International Atomic Energy Agency, Dosimetry in diagnostic radiology: an international code of practice. Vienna: IAEA; 2007. Technical Reports Series No.: 457.

9. Horowitz YS, Satinger D, Fuks E, Oster L, Podpalov L. On the use of LiF:Mg,Ti thermoluminescence dosimeters in space-a critical review. *Radiat Prot Dosimetry* 2003; 106:7-24. doi: 10.1093/oxfordjournals.rpd.a006337.
10. Sadeghi M, Sina S, Faghihi R. Investigation of LiF, Mg and Ti (TLD-100) reproducibility. *J Biomed Phys Eng* 2015;5:217-22.
11. Horowitz Y, Oster L, Eliyahu I. Review of dose-rate effects in the thermoluminescence of LiF: Mg, Ti (HARSHAW). *Radiat Prot Dosimetry* 2018;179:184-8. doi: 10.1093/rpd/ncx248.
12. Hasegawa H, Sato M, Tanaka H. Evaluation of an X-Ray dose profile derived from an optically stimulated luminescent dosimeter during Computed Tomographic Fluoroscopy. *PLoS ONE* 2015;10(7):e0132154. doi: 10.1371/journal.pone.0132154.
13. Choi Y, Shil Cha E, Jin Bang Y, Ko S, Ha M, Lee C, et al. Estimation of organ doses among diagnostic medical radiation workers in South Korea. *Radiat Prot Dosimetry* 2018;179:142-50. doi: 10.1093/rpd/ncx239.
14. Ivanauskaite D, Griociene B. Status of individual dosimetry for dentists in Lithuania in year 1996-2001. *Stomatologija* 2003;5:149-51.
15. Sharma J, Sarma J, Agarwal S. Assessment of diagnostic reference level in radiography of neonatal chest anteroposterior examination: a hospital-based study. *J Med Phys* 2018;43:200-3. doi: 10.4103/jmp.JMP_37_18.
16. Institute of Physical Sciences in Medicine. National protocol for patient dose measurement in diagnostic radiology. Chilton:NRPB;1992.
17. Raffi RA, Davis SD, Hammer CG, Micka JA, Kunugi KA, Musgrove JE; et al. Determination of exit skin dose for ¹⁹²Ir intracavitary accelerated partial breast irradiation with thermoluminescent dosimeters. *Med Phys* 2010;37: 2693-702. doi: 10.1118/1.3429089.

18. Omojola AD, Akpochafor MO, Adeneye SO, Aweda MA. Calibration of MTS N (LiF: Mg, Ti) chips using cesium 137 source at low doses for personnel dosimetry in diagnostic radiology. *Radiat Prot Environ* 2020;43:108-14.
19. Radiation and Nuclear Safety Authority (STUK). Radiation practices and radiation measurements. Helsinki: STUK; 2016.
20. Nilsson B, Sorcini B. Surface dose measurements in clinical photon beams. *Acta Oncol* 1989;28:537-42. doi: 10.3109/02841868909092265.
21. Yusof MFM, Yahya MH, Rosnan MS, Abdullah R, Abdul Kadir AB. Dose measurement using Al₂O₃ dosimeter in comparison to LiF: Mg, Ti dosimeter and ionization chamber at low and high energy X-ray. *AIP Conf Proc* 2017;1799:040007. doi: 10.1063/1.4972931.
22. Herrati A, Bourouina M, Khalal-Kouache K. Investigation of TLD-700 energy response to low energy x-ray encountered in diagnostic radiology. *Open Phys* 2016;14:150-8. doi: 10.1515/phys-2016-0016.
23. Alashrah S, Kandaiya S, Maalej N, El-Taher A. Skin dose measurements using radiochromic films, TLDs and ionisation chamber and comparison with Monte Carlo simulation. *Radiat Prot Dosimetry* 2014;162:338-44. doi: 10.1093/rpd/nct315.
24. Reynolds TA, Higgins P. Surface dose measurements with commonly used detectors: a consistent thickness correction method. *J Appl Clin Med Phys* 2015;16:358-66. doi: 10.1120/jacmp.v16i5.5572.
25. Fitriandini A, Wibowo WE, Pawiro SA. Comparison of dosimeter response: ionization chamber, TLD, and Gafchromic EBT2 film in 3D-CRT, IMRT, and SBRT techniques for lung cancer. *J Phys:Conf Ser* 2016;694:012006. doi: 10.1088/1742-6596/694/1/012006.

26. Waqar M, Ul-Haq A, Bilal S, Mosood M. Comparison of dosimeter response of TLD-100 and ionization chamber for high energy photon beams at KIRAN Karachi in Pakistan. *Egypt J Radiol Nucl Med* 2017; 48 :479-83. doi:10.1016/j.ejrn.2017.01.012
27. Lee JH, Chang LT, Shiau AC, Chen CW, Liao YJ, Li WJ,et al. A novel simple phantom for verifying the dose of radiation therapy. *BioMed Res Int* 2015 ;2015:934387. doi: 10.1155/2015/934387.

Case Report

Mimicker of Fitz-Hugh-Curtis syndrome: A case report of perihepatitis secondary to sigmoid colonic perforation

Sirote Wongwaisayawan, M.D.⁽¹⁾

Pinporn Jenjitranant, M.D.⁽¹⁾

Natthawut Jarunnarumol, M.D.⁽¹⁾

Goragoch Gesprasert, M.D., Ph.D.⁽²⁾

Nitima Saksobhavit, M.D.⁽¹⁾

From ⁽¹⁾ Department of Diagnostic and Therapeutic Radiology, Faculty of Medicine
Ramathibodi Hospital, Mahidol University, Bangkok, Thailand.

⁽²⁾ Department of Surgery, Faculty of Medicine Ramathibodi Hospital,
Mahidol University, Bangkok, Thailand.

Address correspondence to S.W. (e-mail: sirote.won@mahidol.edu)

Received 25 March 2021; revised 11 April 2021; accepted 12 April 2021
doi:10.46475/aseanjr.v22i1.123

Abstract

Perihepatitis is an uncommon condition defined as the inflammation of the peritoneal liver capsule. It is more commonly known as Fitz-Hugh-Curtis syndrome, a rare condition characterized by the inflammation of the peritoneum and tissue around the liver. This syndrome is usually associated with pelvic inflammatory disease (PID). However, PID is not always the cause of perihepatitis. We reported a rare case of perihepatitis which occurs secondarily to sigmoid colonic perforation.

Keywords: Perihepatitis syndrome, Sigmoid colon, Intestinal perforation, Fitz-Hugh-Curtis syndrome.

Introduction

Perihepatitis is an uncommon condition that is defined as the inflammation of the peritoneal liver capsule. It is traditionally described as Fitz-Hugh-Curtis syndrome, a rare condition characterized by secondary inflammation of the peritoneum and tissue around the liver from pelvic inflammatory disease (PID) [1,2]. On a computed tomography (CT) scan, the inflammation of tissue around the liver may be seen as an intense enhancement of the liver capsule. This CT finding can serve as a hint to evaluate the pelvic inflammatory condition, particularly PID or tubo-ovarian abscess (TOA). However, PID or TOA is not always the cause of perihepatitis. This case report presents a rare case of perihepatitis which occurs secondarily to sigmoid colonic perforation.

Case Summary

An 88-year-old woman was presented to the emergency department (ED) with progressive epigastric pain for two days. She denied any nausea, vomiting, and fever. She had a past history of chronic deep venous thrombosis (DVT) of the left leg and a previous hysterectomy with bilateral oophorectomy.

On admission, the patient had a blood pressure of 143/76 mm Hg, a heart rate of 112 bpm, and a body temperature of 36.7 degrees Celcius. The physical examination revealed abdominal distension, decreased bowel sound, generalized guarding, and rebound tenderness in the epigastric area. The laboratory results showed a normal white blood cell count ($8.9 \times 10^9/L$) and an elevated serum lactate level of 5.2 mmol/L (normal range: 0.7-2.5 mmol/L). The serum electrolyte panels and liver function tests were within normal limits.

An emergency contrast-enhanced CT scan at the ED revealed a small amount of perihepatic fluid and conspicuous intense enhancement of the liver capsule along the right hepatic lobe which represents perihepatitis (Figure 1). Segmental colitis with sigmoid colonic perforation, pneumoperitoneum, and

fecal contamination in the peritoneal cavity are noted (Figure 2) and thought to be the causes of abdominal pain in this patient. Peritoneal fat inflammation in the right-sided abdomen is also seen. The patient underwent emergent exploratory laparotomy which revealed a 3-cm sigmoid colonic perforation. Severe fecal contamination and severe adhesion of the entire abdomen were noted intraoperatively (Figure 3). The cause of sigmoid colonic perforation in this patient was presumed to be stercoral colitis. Adhesiolysis and Hartmann's procedure were performed. The patient tolerated the procedure without any immediate postoperative complications. The pathological result confirmed the diagnosis of sigmoid colonic perforation. No malignancy was found in the surgical specimen.

The patient made a satisfactory post-operative recovery in the intensive care unit (ICU) and was discharged from the hospital on postoperative day 23. She had been doing well at her last surgical outpatient follow-up.



Figure 1. Axial contrast-enhanced computed tomography scan showing small amount of perihepatic fluid and intense enhancement of the liver capsule along the right hepatic lobe (arrows).

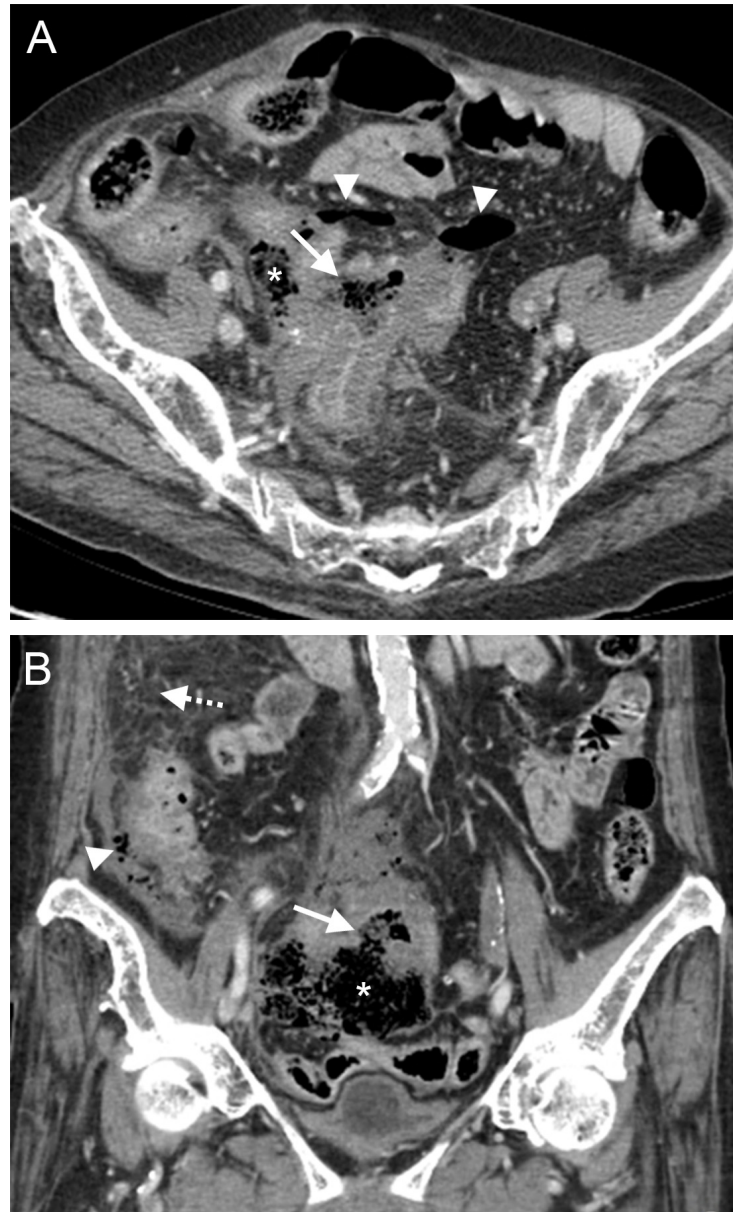


Figure 2. Contrast-enhanced computed tomography scan in axial (A) and coronal (B) views showing sigmoid colonic perforation (arrow) and fecal contamination in the peritoneal cavity (asterisk). Extraluminal free air in the pelvic cavity and right lower quadrant abdomen is observed (arrowheads). Peritoneal fat stranding along the right paracolic gutter is also seen (dashed arrow).

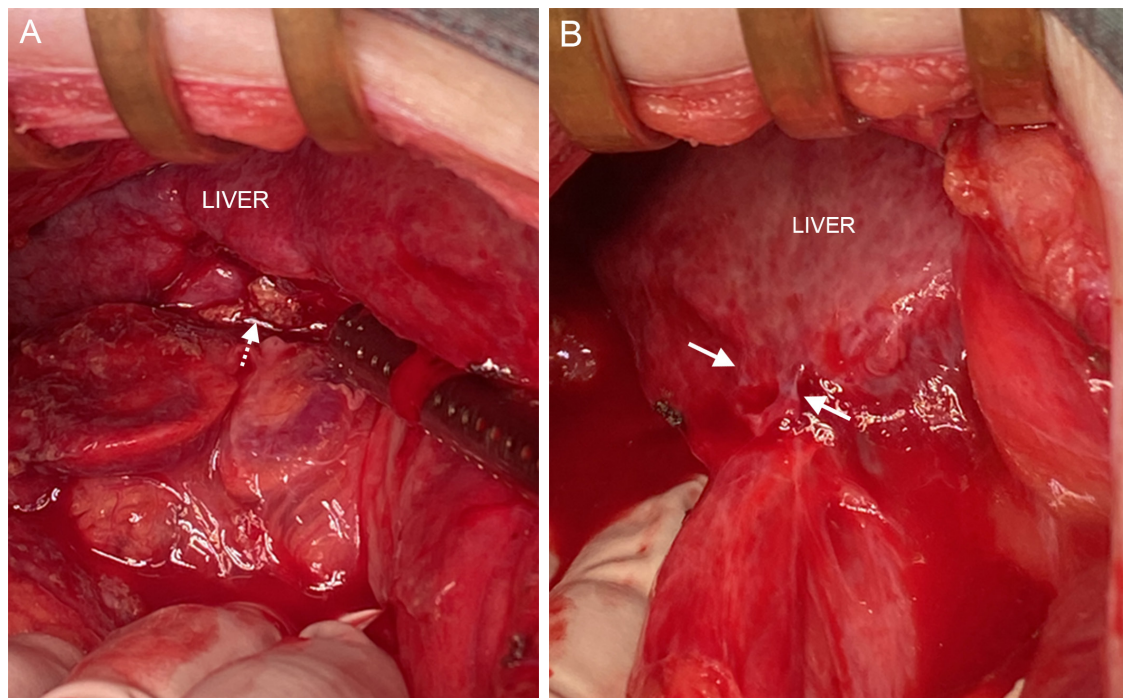


Figure 3. Intraoperative photographs (A, B) showing fecal contamination (dashed arrow) and string-like adhesion (arrows) in the perihepatic space.

Discussion

Perihepatitis is defined as an inflammation of the liver capsule and tissue around the liver, regardless of the involvement of the liver parenchyma. It is classically described in association with the pelvic inflammatory disease (PID) caused by *C. trachomatis* or *N. gonorrhoeae*, the so-called “Fitz-Hugh-Curtis syndrome” [1,2]. Fitz-Hugh-Curtis syndrome is thought to be a result of the intraperitoneal spread of the infection from the pelvic cavity, with associated adhesion formation in the perihepatic region and the right upper quadrant (RUQ) abdomen [3]. The typical presented symptoms include RUQ abdominal pain and tenderness in a young reproductive female. The diagnosis of Fitz-Hugh-Curtis syndrome is usually confirmed by direct visualization of violin string-like adhesions through a laparoscopy or laparotomy, or by positive culture of *C. trachomatis* or *N. gonorrhoeae* in fluid from the pelvic cavity or in a cervical smear [3].

The inflammation and the increased blood flow of the peritoneum may manifest as intense enhancement of the liver capsule on an early-phase or arterial-phase CT image which is described as perihepatitis [4-6].

To our knowledge, this is the first case report of perihepatitis secondary to sigmoid colonic perforation, which mimics the CT findings of Fitz-Hugh-Curtis syndrome. The pelvic inflammation in the present case was a result of the perforated sigmoid colon and intraperitoneal fecal contamination, rather than the classically described PID or TOA in Fitz-Hugh-Curtis syndrome. Although the presented patient did not have a confirmatory test for *C. trachomatis* or *N. gonorrhoeae* infection, the patient reported no active sexual activity and there were no suspicious intraoperative findings of PID or TOA. Moreover, the patient had undergone total hysterectomy many years before this presentation, making the occurrence of PID or TOA very unlikely.

Previous studies had reported 82%-86% overall accuracy of CT scan in predicting the site of bowel perforation [7,8]. In subtle cases, small loculated extraluminal air, pericolic fat stranding, and colonic wall thickening may be the only signs of the perforation site [9]. The presence of perihepatitis can increase the level of confidence in identifying the perforation site because the abnormality in the pelvic cavity is anticipated. The presence of extraluminal bowel content, loculated extraluminal air, bowel wall thickening, and defect of bowel wall in the pelvic cavity should be carefully assessed on CT images [7].

We postulate that the inflammatory fluid and fecal contamination in the pelvic cavity spread to the RUQ abdomen by means of transperitoneal ascitic flow. The peritoneal fluid in the pelvis is drawn to the upper abdomen, particularly at the right subdiaphragmatic region, secondary to the hydrostatic pressure variation from the diaphragmatic movement during inspiration [10]. Therefore, any pelvic inflammatory condition can theoretically result in the secondary inflammation of the perihepatic space or right subphrenic space. A similar finding of intense hepatic capsular enhancement has been reported in a patient with systemic lupus erythematosus [11]. Any condition that causes inflammation of the peritoneum

of the RUQ abdomen may have intense enhancement of the liver capsule as well, such as cholecystitis, hepatic abscess, cholangitis, superior vena cava obstruction, tuberculous peritonitis, exposure of the liver to radiation, peritoneal carcinomatosis, and hepatic schistosomiasis [3]. However, other ancillary findings are usually present in most of these conditions and can serve as clues to the correct diagnosis.

Conclusion

We described a rare cause of perihepatitis resulting from sigmoid colonic perforation. The presence of perihepatitis on a CT scan should raise the possibility of the pelvic inflammatory condition. Therefore, the abnormality in the pelvic cavity should be carefully evaluated on a CT scan. The radiologists' awareness of this condition can help facilitate the correct diagnosis and guide the appropriate treatment.

References

1. Fitz-Hugh T. Jr. Acute gonococccic peritonitis of the right upper quadrant in women. JAMA 1934;102:2094-6.
2. Curtis AH. A cause of adhesions in the right upper quadrant. JAMA 1930;94.1221-2.
3. Kim S, Kim TU, Lee JW, Lee TH, Lee SH, Jeon TY, et al. The perihepatic space: comprehensive anatomy and CT features of pathologic conditions. Radiographics 2007;27:129-43. doi: 10.1148/rg.271065050.
4. Tsubuku M, Hayashi S, Terahara A, Furukawa T, Ohmura G. Fitz-Hugh-Curtis syndrome: linear contrast enhancement of the surface of the liver on CT. J Comput Assist Tomogr 2002;26:456-8. doi: 10.1097/00004728-200205000-00025.
5. Nishie A, Yoshimitsu K, Irie H, Yoshitake T, Aibe H, Tajima T, et al. Fitz-Hugh-Curtis syndrome. Radiologic manifestation. J Comput Assist Tomogr 2003;27:786-91. doi: 10.1097/00004728-200309000-00017.
6. Joo SH, Kim MJ, Lim JS, Kim JH, Kim KW. CT Diagnosis of Fitz-Hugh and Curtis Syndrome: value of the arterial phase scan. Korean J Radiol 2007;8:40-7. doi: 10.3348/kjr.2007.8.1.40.
7. Hainaux B, Agneessens E, Bertinotti R, De Maertelaer V, Rubesova E, Capelluto E, et al. Accuracy of MDCT in predicting site of gastrointestinal tract perforation. AJR Am J Roentgenol 2006;187:1179-83. doi: 10.2214/AJR.05.1179.
8. Catalano O. [Computed tomography in the study of gastrointestinal perforation]. Radiol Med 1996;91:247-52. Italian.

9. Singh JP, Steward MJ, Booth TC, Mukhtar H, Murray D. Evolution of imaging for abdominal perforation. *Ann R Coll Surg Engl* 2010;92:182-8. doi:10.1308/003588410X12664192075251.
10. Pannu HK, Oliphant M. The subperitoneal space and peritoneal cavity: basic concepts. *Abdom Imaging* 2015;40:2710-22. doi: 10.1007/s00261-015-0429-5.
11. Schoenwaelder M, Stuckey SL. Perihepatitis associated with systemic lupus erythematosus: computed tomography findings. *Australas Radiol* 2005;49:179-81. doi: 10.1111/j.1440-1673.2005.01370.x.

Case Report

Pulmonary sclerosing pneumocytoma, an adenocarcinoma mimicker: A case report and review of the literature

Mohd Zulkimi Roslly, M.D.

Aida Widure Mustapha Mohd Mustapha, M.D.

Nik Farhan Nik Fuad, M.D.

From Department of Radiology, Faculty of Medicine, Universiti Kebangsaan Malaysia ,
Malaysia.

Address correspondence to M.Z.R. (e-mail: zulkimiroslly@gmail.com)

Received 18 February 2021; revised 17 April 2021; accepted 17 April 2021
doi:10.46475/aseanjr.v22i1.120

Abstract

Pulmonary sclerosing pneumocytoma (PSP) is a rare condition, occupying only approximately 1% of all benign lung neoplasms and the description of this disease through a radiological perspective is limited. Only approximately a third of PSP has been correctly diagnosed pre-operatively through contrast-enhanced computed tomography (CECT) thorax. To date, only few radiological features have been described to ascertain this disease and there is still a significant portion of patients being misdiagnosed with a malignant neoplasm. We report a case of PSP that was initially misdiagnosed as lung adenocarcinoma stage IIA and the histopathological findings of surgical resection confirmed the diagnosis of PSP. We try to add some points from this case into the previous radiological description of this uncommon disease with a common presentation.

Keywords: Sclerosing, Pneumocytoma, Adenocarcinoma, Pulmonary.

Introduction

Pulmonary sclerosing pneumocytoma (PSP), previously known as pulmonary sclerosing hemangiomas (PSH) is rare, accounting for approximately 1% of all benign lung tumours. It was first described in 1956 by Liebow and Hubbell [1] after several personal observations and analyses of similar cases being reported under different entities including xantoma, histiocytoma and xanthofibroma. Subsequently, the term “sclerosing hemangioma” was selected based on the identical histologic morphology until year 2015 where the World Health Organization (WHO) changed the term “sclerosing hemangioma” to “sclerosing pneumocytoma” under the new classification of lung tumours, after several immunohistochemistry studies [2]. This entity predominantly affects middle-age adults of over 50 years old with 5:1 female to male ratio predilection [3]. To date, only a few radiological features have been described to ascertain this disease and there is still a significant portion of patients being misdiagnosed with a malignant neoplasm. We report a case of PSP that was initially misdiagnosed as lung adenocarcinoma stage IIA and the histopathological findings of surgical resection confirmed the diagnosis of PSP.

Case summary

A 60-year-old lady with hypertension and type 2 diabetes was physically well except mild occasional shortness of breath on exertion. Physical examinations were unremarkable. A routine chest radiograph (CXR) was performed during a regular follow-up for her premorbid condition in a health clinic showed a right lung mass. She was then subject to contrast-enhanced computed tomography (CECT) of the thorax for further evaluation.

The initial chest radiograph (Figure 1) and CECT of the thorax (Figure 2a and 2b) revealed a large well-defined heterogeneous rounded mass at the right perihilar region in the anterior segment of the right upper lobe measuring 6.0x6.5x5.8 cm. The mass displaced the right minor fissure inferiorly and splayed the adjacent vessels and bronchi of the right hilum. There was no evidence of distant metastasis.

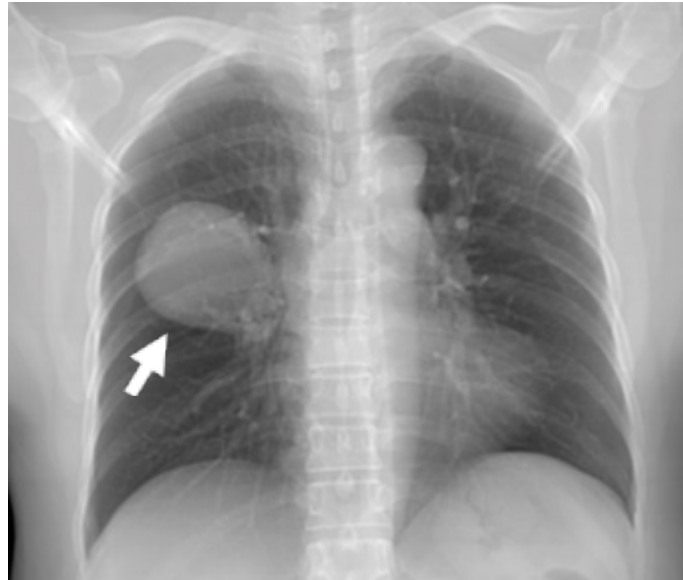


Figure 1. Frontal chest radiograph reveals a well-defined mass at right perihilar region (arrow).

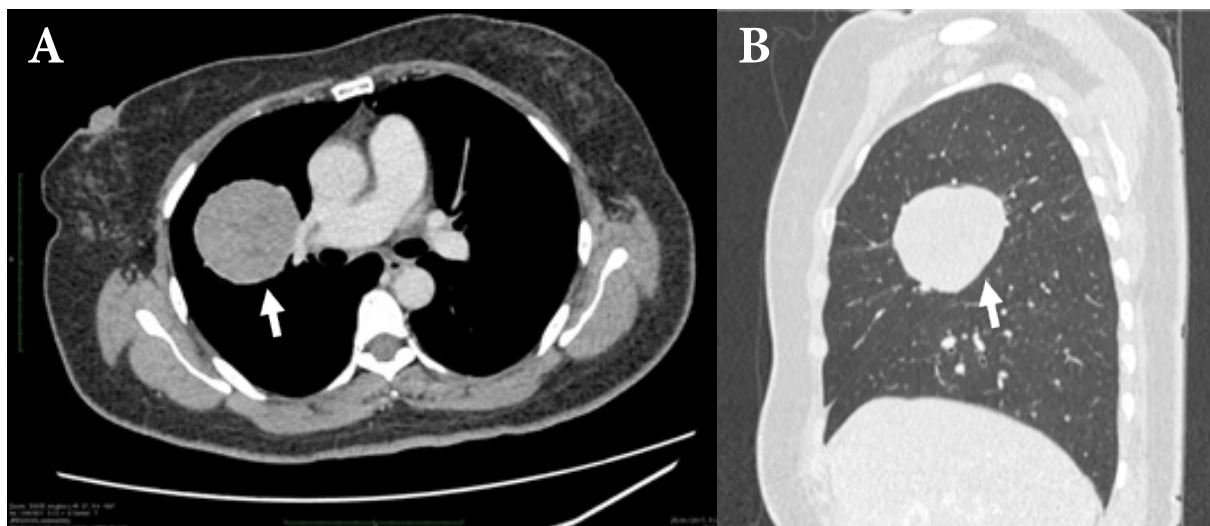


Figure 2. Axial image of contrast-enhanced CT (a) and sagittal image in lung window (b) show a well-defined heterogeneously enhancing lung mass at right perihilar region. (arrows).

Bronchoscopy showed the anterior segment of the right upper lobe bronchus slightly compressed by mass but did not obstruct the lumen and there was no endobronchial mass detected. A core-needle biopsy was performed under the CT-guidance and the histopathological report showed lung adenocarcinoma stage IIA. The core biopsy showed positivity towards thyroid transcription factor-1 (TTF-1) but proved inconclusive for cytokeratin-7 (CK7). Cytokeratin-20 (CK 20) stain was not available in the laboratory; however, the overall conclusion of the core biopsy being adenocarcinoma in the right lung was made based on the TTF-1 positivity. She developed chesty cough and constitutional symptoms a few weeks later and was treated accordingly.

CECT of the thorax, abdomen and pelvis was performed four months later for restaging which showed a well-defined heterogenous perihilar lung parenchymal mass in the anterior segment of the right upper lobe with no significant change in size as the previous CECT findings. The lesion was located 5.2 cm from the carina and caused splaying with mild narrowing of the right upper bronchus and bronchus intermedius with the patent bronchial lumen. Postero-inferiorly, it was abutting the right oblique fissure. It showed average attenuation of +44 HU with a maximum enhancement of +57 HU. There was no fat-attenuating component or calcification shown within the mass. The presence of subcentimeter right paratracheal lymph node was detected. The overall CECT findings concluded that this patient was in stage T2N0Mx of lung carcinoma. Fluorine-18 fluorodeoxyglucose positron emission tomography CT (¹⁸F-FDG PET/CT) was also performed for complete assessment. It showed a heterogeneously hypermetabolic mass with SUV_{max} of 5.5. Core-needle biopsy was repeated. The overall histopathological study reported adenocarcinoma of the right lung.

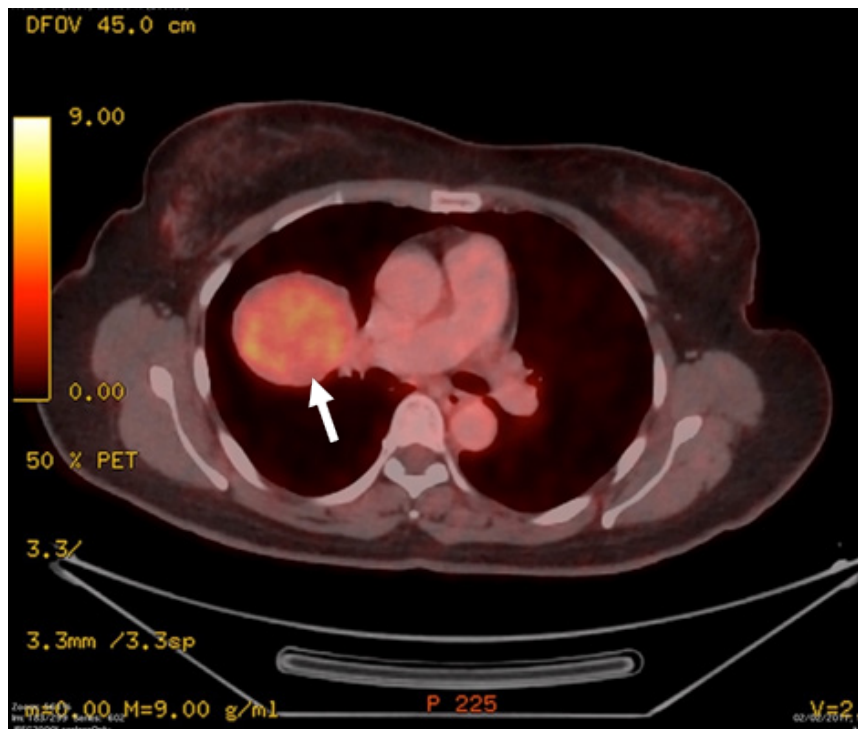


Figure 3. ¹⁸F-FDG PET/CT image in axial view shows a heterogeneously hypermetabolic right perihilar mass with SUV_{max} of 5.5 (arrow).

The patient then was subject to thoracotomy and bilobectomy of the right upper and middle lobes. Intraoperatively, approximately 6 cm of haemorrhagic tumour was noted at the right upper lobe invading the middle lobe. The adjacent lymph nodes were also sampled. Surgical specimens were seen 15 mm from the nearest bronchial margin and 10 mm from the parenchymal margin. Microscopically, it showed a circumscribed tumour comprising two populations of neoplastic cells: the cuboidal surface cells and the stromal round cells. Also, mitotic figure was rarely seen (Figure 4). Further immunohistochemistry showed the final diagnosis of sclerosing pneumocytoma in the right lung.

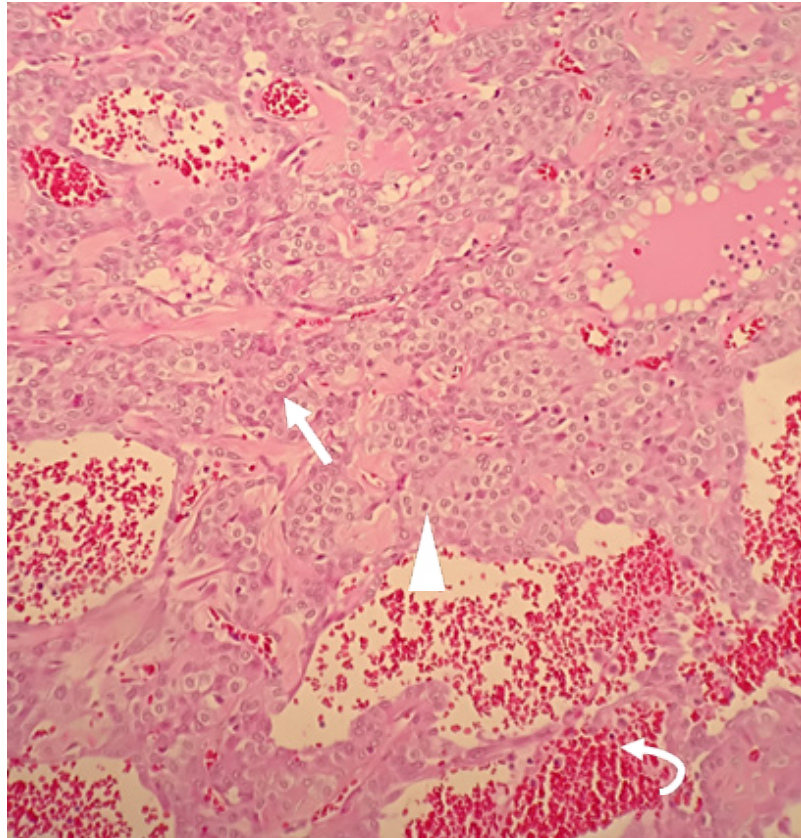


Figure 4. Hematoxylin and Eosin staining of the surgical specimen shows two populations of neoplastic cells: the cuboidal surface cells (arrow) and the stromal round cells (arrowhead) with patchy areas of the hemorrhagic component (curved arrow).

The patient was diagnosed with hospital-acquired pneumonia post-operatively but discharged well 17 days post-op after being treatment. Currently, the patient is doing well at home and asymptomatic.

Discussion

PSP was mainly found incidentally in around 70% of the patients [2, 4, 5]. Referring to our case, the mass was found during a regular follow up chest radiograph. A smaller number of patients may present with non-specific symptoms like hemoptysis, chronic cough, and chest pain.

The most common presenting form is an asymptomatic solitary pulmonary nodule that can grow up to 7 cm in diameter. Although 73% of the lesions are smaller than 3 cm [2], PSP is usually found as a moderate-size lesion with the diameter sizes of the tumours ranging from 2.5–6.5 cm [6]. Most patients manifest with a single lesion, accounting for 92.1% as reported by Shin SY et al. [4]. This finding is consistent with a study done by Wang et al. [7] whereby 100% of the patients had a single pulmonary lesion. Yang Lei et al. [8] reported 96% of the patients found to have a solitary lung mass irrespective of the location which were mainly round in shape. Our case appeared to be compatible with the findings in both of these studies.

In a study by Cheung YC et al.[6], all of the PSP appeared to be located in the perihilar region with all lesions smoothly encapsulated. He also reported that all PSP appeared to be located at the perihilar region. In a study by Wang QB et al [7], PSP appeared as a well-defined mass and was generally a juxtapleural mass in 94% of the patients on the CT. As found by Wang Q.B [7] and Im JG et al. [9], the PSP was found as a juxtapleural mass in 94% and 100% of the patients, respectively. Our case showed that the mass was located 5.2 cm from the carina based on the CECT thorax and lay 1.0 cm from the parenchymal margin.

According to Cheung Y et al. [6], in terms of the contrast enhancement pattern, the majority of the patients had heterogeneous enhancement with HU ranging from +67 to +112 HU. The mean CT attenuation of the lesions from 76 patients was +76 (+/-47.1) (range, 0–150.3) HU. Heterogeneous attenuation was more common (59.0%) in CECT studies [4]. In our case, the enhancement pattern of the mass was fairly heterogenous. The average attenuation of the mass was

+44 HU; with the minimum and maximum enhancement attenuation of +40HU and +57 HU, respectively which corresponded to the studies conducted earlier. However, the non contrast-enhanced study was not performed in our case according to the local scanning protocol. There was no area with fat-attenuation or calcification within the mass. Neither were there areas of fluid-attenuation to suggest a liquified or necrotic component. In contrast to a study by Wang QB et al.[7], the attenuation of post enhancement was found to be higher at +79 (+/-3) HU and homogenous in 75% of the patients. They also concluded that the diameter of the heterogeneously enhanced tumour was larger than that of the homogeneously enhanced tumours. On a CT-pathology correlation, the higher, equal, or lower attenuation areas correspond with angiomatous, solid and sclerotic, and cystic areas, respectively [9].

Based on a relatively large retrospective study by Shin SY et al. [4] of 76 patients with confirmed of PSP, 4 specific CT signs were identified. They are marginal pseudocapsule sign, overlying vessel sign, air-gap sign and halo sign. However, none of these signs were present in our case. The majority of patients presented a peripheral, solitary lesion with smooth margins [8].

PSP classically is a histological diagnosis and correct diagnosis on the formal radiologic report of the conventional chest CECT is possible in only 30.3% of 76 patients [5]. Its CECT manifestation varies according to the composition [6].

¹⁸F-FDG PET hypometabolic uptake of PSP mass was evident in a study by Shin SY et al. [4] that showed 17 patients who underwent ¹⁸F-FDG PET showing a hypo- or intermediate metabolic lesion. This was in contrast to several studies performed on the FDG uptake of PSP such as by Lin KH et al. [10] where they found that the maximal standard uptake value (SUVmax) of FDG uptake was positively correlated with the tumour size. This shows that a larger PSH has a higher uptake and might be misrecognized as a malignancy. In our case, the mass was considered a large mass (>5cm), thus, demonstrating a hypermetabolic activity on ¹⁸F-FDG PET.

Conclusion

We report a case of PSP which was initially diagnosed as lung adenocarcinoma. PSP is a rare benign lung tumour and tissue diagnosis is the gold standard investigation. The radiological description and diagnosis remain difficult and there is no definitive diagnostic radiological finding of PSP which might lead to misdiagnosis and unnecessary surgical intervention with the patient. However, the clinical and radiological characteristics of the mass described in our case and in the literature may guide the reporting radiologist to infer this diagnosis in the list of differential diagnosis.

References

1. Liebow AA, Hubbell DS. Sclerosing hemangioma (histiocytoma, xanthoma) of the lung. *Cancer* 1956;9:53-75. doi:10.1002/1097-0142(195601/02)9:1<53::aid-cncr2820090104>3.0.co;2-u.
2. Devouassoux-Shisheboran M, Hayashi T, Linnoila RI, Koss MN, Travis WD. A clinicopathologic study of 100 cases of pulmonary sclerosing hemangioma with immunohistochemical studies: TTF-1 is expressed in both round and surface cells, suggesting an origin from primitive respiratory epithelium. *Am J Surg Pathol* 2000 ;24:906-16. doi: 10.1097/00000478-200007000-00002.
3. Neuman J, Rosioreanu A, Schuss A, Turi G, Yung E, Trow TK, et al. Radiology-pathology conference: sclerosing hemangioma of the lung. *Clin Imaging* 2006;30:409-12. doi: 10.1016/j.clinimag.2006.05.030.
4. Shin SY, Kim MY, Oh SY, Lee HJ, Hong SA, Jang SJ, et al. Pulmonary sclerosing pneumocytoma of the lung: CT characteristics in a large series of a tertiary referral center. *Medicine (Baltimore)* 2015;94:e498. doi: 10.1097/MD.0000000000000498.
5. Sugio K, Yokoyama H, Kaneko S, Ishida T, Sugimachi K. Sclerosing hemangioma of the lung: radiographic and pathological study. *Ann Thorac Surg* 1992 ;53:295-300. doi: 10.1016/0003-4975(92)91336-8.
6. Cheung YC, Ng SH, Chang JW, Tan CF, Huang SF, Yu CT. Histopathological and CT features of pulmonary sclerosing haemangiomas. *Clin Radiol* 2003 ;58:630-5. doi: 10.1016/s0009-9260(03)00177-6.
7. Wang QB, Chen YQ, Shen JJ, Zhang C, Song B, Zhu XJ, et al. Sixteen cases of pulmonary sclerosing haemangioma: CT findings are not definitive for preoperative diagnosis. *Clin Radiol* 2011;66:708-14. doi: 10.1016/j.crad.2011.03.002.

8. Lei Y, Yong D, Jun-Zhong R, Zhi Y, Zi-Tong W. Treatment of 28 patients with sclerosing hemangioma (SH) of the lung. *J Cardiothorac Surg* 2012;7:34. doi: 10.1186/1749-8090-7-34.
9. Im JG, Kim WH, Han MC, Han YM, Chung JW, Ahn JM, et al. Sclerosing hemangiomas of the lung and interlobar fissures: CT findings. *J Comput Assist Tomogr* 1994;18:34-8. doi: 10.1097/00004728-199401000-00007.
10. Lin KH, Chang CP, Liu RS, Wang SJ. F-18 FDG PET/CT in evaluation of pulmonary sclerosing hemangioma. *Clin Nucl Med* 2011;36:341-3. doi: 10.1097/RLU.0b013e31820aa00c.

ASEAN Movement in Radiology

The Royal College of Radiologists of Thailand in collaboration with Thailand Center of Excellence in Life Sciences shape the future of artificial intelligence in diagnostic radiology

Sitthichok Chaichulee, Ph.D.⁽¹⁾

Thammasin Ingvaya, M.D., Ph.D.⁽²⁾

Supharerk Thawillarp, M.D., D.P.H.⁽³⁾

Pattarawin Attasara, M.D.⁽⁴⁾

Wiwatana Tanomkiat, M.D.⁽⁵⁾

From ⁽¹⁾ Department of Biomedical Sciences and Biomedical Engineering,
⁽²⁾ Department of Family and Preventive Medicine,
⁽⁵⁾ Department of Radiology, Faculty of Medicine, Prince of Songkla University,
Hat Yai, Songkhla, 90110, Thailand.
⁽³⁾ Epidemic Intelligence Unit (EIU), Department of Disease Control,
Ministry of Public Health, Nonthaburi, 11000, Thailand.
⁽⁴⁾ Digital Medical Bureau, Medical Services Department, Ministry of Public Health,
Nonthaburi, 11000, Thailand.
Address correspondence to W.T. (email: twiwadha@hotmail.com)

Received 21 April 2021; accepted 25 April 2021
doi:10.46475/aseanjr.v22i1.126

Keywords: Artificial intelligence, AI, Diagnostic Radiology, Thailand.

The COVID-19 pandemic has disrupted the traditional way of living in almost all aspects. Physical distancing was suggested, and partial lock-down policies have been implemented. The development and uses of technology are being accelerated to overcome the massive obstacle for humankind, or even to eliminate this fatal infection.

Before the pandemic, tuberculosis (TB) has long been a major health problem in Thailand throughout its 800 years of history or longer. Currently, Thailand has been classified by the World Health Organization (WHO) as one of the 22 countries in the world with the highest TB burden. As the number one cause of death amongst infectious diseases at the global level, more prominent than AIDS, the United Nation (UN) and WHO have listed TB control as part of their Sustainable Development Goals (SDGs). With the TB incidence of 1.3 times the global rate, Thailand is committed to decrease new cases to less than 10 per 100 000 population within 2025 [1]. To achieve this highly challenging goal, all actively infected cases will have to be found and treated. Since TB commonly attacks persons who are usually in a weakened condition or living in a confined space, Thailand's case-finding strategy is currently applied with 7 high-risk groups including persons who have contact with patients diagnosed with TB, HIV-infected patients, diabetic patients with poor glycemic control, aged persons with chronic diseases, prisoners, migrant workers, and health care providers. Because of its high sensitivity, the chest radiograph is used as a screening tool for these 7 high-risk groups, regardless of their symptoms. The screening campaign has included the prisoners in 2017. The people in the other 6 high-risk groups will be covered by 2021. A rapid increase in the uses of chest radiographs is expected. The interpretation of the large volume of chest radiographs will be a heavy burden to radiologists. In addition, since the interpretation by radiologists is not timely made, patients will probably be detected in a delayed manner, especially when their chest radiographs are abnormal. AI is expected to triage and screen the normal films at the site.

Several AIs have been developed for reading chest radiographs. They are either imported or locally invented. While AI seems to be a good prospect in assisting the medical team, there remain many questions to be answered. The sensitivity of disease detections, the experience and feeling of the patients and the service providers, safety and security of patients' data, changes that might disrupt the hospital workflow and the structure of the radiology unit, the sustainability and fairness to the buyers and more, are some examples. Doubts in the usefulness and adverse reactions of AIs will lead to reluctance in the development of new AI algorithms.

To support the AI users, the Royal College of Radiologists of Thailand (RCRT) has developed the AI user guideline covering all essential points to help users make an informed decision regarding the purchase and uses of AI products. The guideline could help the users understand the problem they are trying to solve, assess whether the AI product is an appropriate solution for their organization, interpret the performance claims made by the vendor, assure whether the product meets regulatory, safety and ethical standards, ensure whether the processing of data fully complies with the organizational data privacy policy, thus, promoting the sustainable use of AI in the organization. It is believed that this guideline will increase the confidence in both users in purchasing the products and inventors and vendors in providing services and products to healthcare providers.

TCELS, under the supervision of the Ministry of Higher Education, Science, Research and Innovation, is a public organization to promote research and innovation in healthcare. TCELS forms networks and shares the resources with many organizations in public, private and non-profit sections. The press release and conference of the collaboration between the 2 organizations and the introduction of AI user guideline was held on April 7, 2021 at Vie Hotel, Bangkok among TCELS alliance and RCRT board.



Figure 1. Mr.Sirasak Teparkum, the TCELS chief executive officer and Associate Professor Wiwatana Tanomkiat, the RCRT president show the memoirs of understanding in collaboration at the press conference.



Figure 2. Dr. Supharek Thawillarp as the representative of the RCRT board, explains how the guideline is developed to the audience in the press conference.



Figure 3. *Dr.Thammasin Ingviya and Dr.Sittichok Chaichulee as the representative of RCRT board give a virtual talk about the plan to develop standard sets of radiographs to test AI.*



Figure 4. *Dr.Pattarawin Attasara as a representative of RCRT board explains the current situation of tuberculosis, the development and use of AI in public health services, and the national policy to end tuberculosis.*

Our next step is to develop a test dataset of Thai chest radiographs, each of which is accurately labelled according to ILO (International Labour Office) classification by B readers who are rigorously certified by the National Institute for Occupational Safety and Health (NIOSH) and specialize in the interpretation of chest radiography. This dataset could serve as a reference for the testing of AI products.

References

1. Bureau of Tuberculosis. Thailand operational plan to end tuberculosis 2017-2021 [Internet]. Nonthaburi: The Bureau; 2017 [cited 2021 Apr 21]. Available from: https://www.tbthailand.org/download/Manual/Thailand%20Operational%20Plan%20To%20End%20%20TB_2017_2021.pdf

Acknowledgement of Reviewers

Reviewer acknowledgement, 2020

Wiwatana Tanomkiat, M.D.

Editor-in-Chief
The ASEAN Journal of Radiology

The editor-in-chief of The ASEAN Journal of Radiology would like to thank all our reviewers who have contributed to the journal during the period from 1 May 2019 through 31 December 2020.

Reviewers

- | | |
|-----------------------------|--------------------------------------------------------------------|
| 1. Anchali Krisanachinda | Chulalongkorn University, Thailand |
| 2. Arthur Edward Brown | Mahidol University, Thailand |
| 3. Chayanin Nitiwarangkul | Mahidol University, Thailand |
| 4. Juntima Euathrongchit | Chiang Mai University, Thailand |
| 5. Keerati Hongsakul | Prince of Songkla University, Thailand |
| 6. Kitiwat Khamwan | Chulalongkorn University, Thailand |
| 7. Kobkun Muangsomboon | Mahidol University, Thailand |
| 8. Krisna Dissaneevate | Rajavithi Hospital, Thailand |
| 9. Linda Brown | Mahidol University, Thailand |
| 10. Napapong Pongnapang | Mahidol University, Thailand |
| 11. Nucharin Supakul | Indiana University School of Medicine,
United States of America |
| 12. Nuttaya Pattamapaspong | Chiang Mai University, Thailand |
| 13. Nuttha Sanghan | Prince of Songkla University, Thailand |
| 14. Panruethai Trinavarat | Chulalongkorn University, Thailand |
| 15. Pattira Boonsri | Prince of Songkla University, Thailand |
| 16. Pawanrat Kranokpiraksa | Chulalongkorn University, Thailand |
| 17. Polpat Soponsakulrat | T&A Gallery, Thailand |
| 18. Pramot Tanutit | Prince of Songkla University, Thailand |
| 19. Rathachai Kaewlai | Mahidol University, Thailand |
| 20. Saowanee Srirattanapong | Mahidol university, Thailand |

Acknowledgement of Reviewers

21. Siriporn Hirunpat	Prince of Songkla University, Thailand
22. Supawitoo Sookpeng	Naresuan University, Thailand
23. Supika Kritsaneepaiboon	Prince of Songkla University, Thailand
24. Sutarat Tungsagunwattana	Central Chest Institute, Thailand
25. Sutipong Jongjirasiri	Mahidol University, Thailand
26. Tanop Srisuwan	Chiang Mai University, Thailand
27. Teeranan Laohawiriyakamol	Prince of Songkla University, Thailand
28. Teeravut Tubtawee	Prince of Songkla University, Thailand
29. Thitiporn Suwatanapongched	Mahidol University, Thailand
30. Yutthaphan Wannasopha	Chiangmai University, Thailand
31. Warawut Sukkasem	Mahidol University, Thailand

ASEAN

This journal provide 4 areas of editorial services: language editing, statistical editing, content editing, and complete reference-citation check in 8 steps:

Step	Services to authors	Services providers
I	Manuscript submitted	Editor
II	Language editing/ A reference-citation check	Language consultant/Bibliographer
III	First revision to ensure that all information remains correct after language editing	Editor
IV	Statistical editing	Statistical consultant
V	Content editing*	Two reviewers
VI	Second revision	Editor
VII	Manuscript accepted/ rejected	Editor/Editorial board
VIII	Manuscript published	Editorial office

*Content editing follows a double-blind reviewing procedure

JOURNAL OF RADIOLOGY